J. Fluid Mech. (2006), *vol.* 551, *pp.* 357–385.
doi:10.1017/S0022112005008402 Printed in the United Kingdom

Sedimentation of an ellipsoid inside an infinitely long tube at low and intermediate Reynolds numbers

By T. N. SWAMINATHAN, K. MUKUNDAKRISHNAN AND HOWARD H. HU†

Department of Mechanical Engineering and Applied Mechanics, University of Pennsylvania, 229 Towne Building, 220 S. 33rd Street, Philadelphia, PA 19104-6315, USA

(Received 18 November 2004 and in revised form 18 August 2005)

The motion of a heavy rigid ellipsoidal particle settling in an infinitely long circular tube filled with an incompressible Newtonian fluid has been studied numerically for three categories of problems, namely, when both fluid and particle inertia are negligible, when fluid inertia is negligible but particle inertia is present, and when both fluid and particle inertia are present. The governing equations for both the fluid and the solid particle have been solved using an arbitrary Lagrangian-Eulerian based finite-element method. Under Stokes flow conditions, an ellipsoid without inertia is observed to follow a perfectly periodic orbit in which the particle rotates and moves from side to side in the tube as it settles. The amplitude and the period of this oscillatory motion depend on the initial orientation and the aspect ratio of the ellipsoid. An ellipsoid with inertia is found to follow initially a similar oscillatory motion with increasing amplitude. Its orientation tends towards a flatter configuration, and the rate of change of its orientation is found to be a function of the particle Stokes number which characterizes the particle inertia. The ellipsoid eventually collides with the tube wall, and settles into a different periodic orbit. For cases with non-zero Reynolds numbers, an ellipsoid is seen to attain a steady-state configuration wherein it falls vertically. The location and configuration of this steady equilibrium varies with the Reynolds number.

1. Introduction

The study of the motion of non-spherical particles in a viscous fluid has a long history. Jeffery (1992) solved the motion of a free ellipsoid in various types of unbounded flow under Stokes flow conditions, and also examined the effective viscosity of a suspension of ellipsoidal particles as a function of particle concentration, ellipticity and orientation. Cox (1965) investigated the steady motion of a particle of arbitrary shape at small Reynolds numbers. He considered two types of problem, one of an arbitrarily shaped body undergoing pure translation in an infinite fluid, and the other of an axially symmetric body in rotation about its axis, combined with translation. The force and torque on the body were derived as an expansion in the Reynolds number. A freely falling spheroid is shown to orientate itself so that its broad-side is perpendicular to the direction of motion. Wakiya (1957) considered the

† Author to whom correspondence should be addressed: hhu@seas.upenn.edu.

motion of a spheroid in the presence of boundary walls under Stokes flow conditions. Using a method of superposition, the expressions for the force and torque on a spheroid were evaluated numerically for two cases. The first one is a spheroid (axis of symmetry parallel to direction of flow) moving between two parallel plates, and the second is a spheroid moving in a tube with its axis of revolution along the axis of the tube.

Broday *et al.* (1998), while examining the motion of non-neutrally buoyant spheroidal particles in vertical unbounded shear flows under creeping-flow conditions, presented a detailed literature review of the study of the motion of non-spherical particles. They calculated the hydrodynamic forces and moments acting on spheroidal particles. Particles with inertia are found to migrate across streamlines, and their trajectories differ considerably from those of the inertialess particles. Sugihara-Seki studied numerically the motions of an inertialess elliptical particle in a channel flow (1993) and that of an ellipsoidal particle in a tube flow (1996). He used a finite-element method to solve the Stokes equations for flow around a spheroid placed at various positions in the tube. The instantaneous velocity was used to compute the particle trajectories. The results from his study have been used in this work to validate our numerical solver. Liu, Bau & Hu (2004) studied, both theoretically and experimentally, the sedimentation of a short cylinder inside a long circular tube in the low-Reynolds-number limit. Bi-cylindrical coordinates were used to derive an analytical expression for how a long guided eccentric cylinder will move along the tube. They found that an off-centred cylinder experiences a torque which causes it to follow an oscillatory trajectory. Their experiments appeared to suggest that the amplitude of the oscillation decays. However, their two-dimensional numerical simulations indicated constant-amplitude oscillations. The issue of whether the oscillatory motion is damped was not resolved.

Russel *et al.* (1977) derived the motion of an inertialess rod-like object falling near a flat wall in Stokes flow. They found that, depending on the initial orientation, the rod can perform two kinds of motion near the wall. A rod approaching near a vertical orientation turns smoothly through the vertical and drifts away with the same end leading which is termed a 'glancing motion', while at orientations close to the horizontal, the wall primarily retards the near end of the rod, causing it to pivot and move away with the opposite end leading, which is termed a 'reversing' motion. It was shown using a lubrication theory, that the end of the rod touches the wall at intermediate orientations. They concluded that between two parallel plates, the rod undergoes a periodic motion. Experiments confirming the theoretical analysis were also performed. An analysis by Caswell (1972) based on a far-field approximation, predicts that the dividing orientation between these two motions of the particle is 45°.

In this paper, the authors have used direct numerical simulations (DNS) to investigate the motion of an ellipsoid settling in an infinitely long circular tube, under the influence of gravity, at low and intermediate Reynolds numbers. The issue of damping of the oscillatory motion for different cases of particle inertia has been examined. The application of DNS to obtain solutions for the motion of solid objects undergoing complex motions in fluids has been well established (Hu, Patankar & Zhu 2001). The use of an arbitrary Lagrangian-Eulerian (ALE) scheme, coupled with a body-fitted moving finite-element mesh, to simulate the motion of moving particles has been documented by Hu and coworkers (1996, 1992, 2001). Previous numerical ALE results on the motion of particles were restricted to spheres because of the inherent complexities introduced by asymmetric objects. In this work, the method established by Hu *et al.* (2001) has been modified and extended to capture the motion of ellipsoids. Section 2 describes the numerical techniques used in the

finite-element scheme; following which the set-up of the problem is described. The final section presents the numerical results obtained from the various simulations and the discussion of those results.

2. Numerical method and meshing

The fluid motion in an inertial frame satisfies the conservation of mass,

$$\nabla \cdot \boldsymbol{u} = 0, \tag{1}$$

and conservation of momentum,

$$\rho_f \left(\frac{\partial \boldsymbol{u}}{\partial t} + (\boldsymbol{u} \cdot \nabla)\, \boldsymbol{u} \right) = -\nabla p + \mu \nabla^2 \boldsymbol{u}, \tag{2}$$

where, $\boldsymbol{u}$ is the fluid velocity vector, μ is the viscosity, ρ_f is the fluid density, and p is the dynamic pressure which is obtained by subtracting the gravitational head from the total pressure.

Consider a suspension of N particles. For the ith particle, particle translation in an inertial frame of reference satisfies the Newton equation given by,

$$m_i \frac{\mathrm{d}\boldsymbol{U}_i}{\mathrm{d}t} = \boldsymbol{F}_i + \boldsymbol{G}_i, \tag{3}$$

$$\frac{\mathrm{d}\boldsymbol{X}_i}{\mathrm{d}t} = \boldsymbol{U}_i, \tag{4}$$

where

$$\boldsymbol{F}_i = \int_{\partial \Gamma_i} \boldsymbol{\sigma} \cdot \hat{\boldsymbol{n}}\, \mathrm{d}S, \tag{5}$$

$$\boldsymbol{\sigma} = -p\boldsymbol{I} + \mu \left[\nabla \boldsymbol{u} + (\nabla \boldsymbol{u})^T \right], \tag{6}$$

$$\boldsymbol{G}_i = (m_i - m_f)\boldsymbol{g}, \tag{7}$$

where $\boldsymbol{U}_i$ is the particle velocity, $\boldsymbol{X}_i$ is the position of the centroid of the ith particle, $\boldsymbol{F}_i$ is the hydrodynamic force exerted by the fluid on the particle, $\boldsymbol{G}_i$ is the effective weight of the particle, m_i is the mass of the ith particle, m_f is the gravitational buoyancy term, and $\boldsymbol{g}$ is the acceleration due to gravity. Also, $\partial \Gamma_i$ is the surface of the ith particle, and $\hat{\boldsymbol{n}}$ is the outward unit vector on the particle surface (pointing into the fluid). For the rotational part of the motion for the ith particle, the Euler equation is given by

$$\frac{\mathrm{d}\left({}^{L}\boldsymbol{I}_i \boldsymbol{\omega}_i\right)}{\mathrm{d}t} = {}^{I}\boldsymbol{C}_i, \tag{8}$$

$$\frac{\mathrm{d}\boldsymbol{\Theta}_i}{\mathrm{d}t} = \boldsymbol{\omega}_i, \tag{9}$$

where ${}^{L}\boldsymbol{I}_i$ is the moment of inertia tensor expressed in the inertial frame, $\boldsymbol{\omega}_i$ is the angular velocity of the ith particle as observed in the inertial frame, ${}^{I}\boldsymbol{C}_i$ is the hydrodynamic moment vector, and $\boldsymbol{\Theta}_i$ is the angular position (Euler angles). The hydrodynamic moment vector, ${}^{I}\boldsymbol{C}_i$ is given by:

$${}^{I}\boldsymbol{C}_i = \int_{\partial \Gamma_i} (\boldsymbol{x} - \boldsymbol{X}_i) \times (\boldsymbol{\sigma} \cdot \hat{\boldsymbol{n}})\, \mathrm{d}S, \tag{10}$$

where $\boldsymbol{\sigma}$ is the hydrodynamic stress tensor given by equation (6), and $\boldsymbol{x}$ is the position vector of a point on the surface of the ith particle.

The moment of inertia tensor, ${}^{L}\boldsymbol{I}_i$, is a 3×3 matrix with six independent components that vary with time as the particle rotates. It is possible to choose a reference frame (principal frame) attached to the body in which ${}^{L}\boldsymbol{I}_i$ can be diagonalized. Using standard vector relations, we can derive the following relation between the rate of change of the angular momentum ${}^{L}\boldsymbol{I}_i\boldsymbol{\omega}_i$ in an inertial frame and that in the body fixed principal frame $\boldsymbol{I}_i\boldsymbol{\Omega}_i$, where $\boldsymbol{I}_i$ is the diagonal moment of inertia tensor, $\boldsymbol{\Omega}_i$ is the angular velocity vector of the rigid body as observed in the body fixed principal frame

$$\frac{{}^{I}\mathrm{d}\left({}^{L}\boldsymbol{I}_i\boldsymbol{\omega}_i\right)}{\mathrm{d}t} = \boldsymbol{I}_i\frac{\mathrm{d}\boldsymbol{\Omega}_i}{\mathrm{d}t} + \boldsymbol{\Omega}_i \times (\boldsymbol{I}_i\boldsymbol{\Omega}_i)\,, \tag{11}$$

where ${}^{I}\mathrm{d}/\mathrm{d}t$ denotes time derivatives on the inertial frame. In equation (11), all the quantities in the right-hand side are expressed in the body fixed frame. Using equation (11) in equation (8), we can derive the modified Euler equation expressed in a body fixed frame as given by:

$$\boldsymbol{I}_i\frac{\mathrm{d}\boldsymbol{\Omega}_i}{\mathrm{d}t} + \boldsymbol{\Omega}_i \times (\boldsymbol{I}_i\boldsymbol{\Omega}_i) = \boldsymbol{C}_i, \tag{12}$$

where $\boldsymbol{C}_i$ is now the hydrodynamic moment vector as expressed in the body fixed frame.

Quaternions (Chou 1992; Kuipers 1999) can be used to represent the orientation of the rigid body. Every orientation can be identified with a rotation about some unit vector $\boldsymbol{a} = (a_1, a_2, a_3)^T$ by an angle γ. The matrix corresponding to this rotation is given by

$$\boldsymbol{R} = \cos\gamma\boldsymbol{I} + (1-\cos\gamma)\begin{bmatrix} a_1{}^2 & a_1a_2 & a_1a_3 \\ a_2a_1 & a_2{}^2 & a_2a_3 \\ a_3a_1 & a_3a_2 & a_3{}^2 \end{bmatrix} + \sin\gamma\begin{bmatrix} 0 & -a_3 & a_2 \\ a_3 & 0 & -a_1 \\ -a_2 & a_1 & 0 \end{bmatrix}, \tag{13}$$

where $\boldsymbol{I}$ is the identity matrix. This orientation can also be represented by the unit quaternion $\boldsymbol{q} = (q_0; q_1, q_2, q_3)$ by setting $q_0 = \cos(\gamma/2)$, $q_i = a_i \sin(\gamma/2)$, $i = 1, 2, 3$. Then the rotation matrix becomes

$$\boldsymbol{R} = \begin{bmatrix} 2\left(q_0^2 + q_1^2\right) - 1 & q_1q_2 - q_0q_3 & q_1q_3 + q_0q_2 \\ q_1q_2 + q_0q_3 & 2\left(q_0^2 + q_2^2\right) - 1 & q_2q_3 - q_0q_1 \\ q_1q_3 - q_0q_2 & q_2q_3 + q_0q_1 & 2\left(q_0^2 + q_3^2\right) - 1 \end{bmatrix}. \tag{14}$$

This orthogonal rotation matrix, $\boldsymbol{R}$, maps vectors in the body fixed frame to vectors in inertial or laboratory fixed frame. Hence, the following relations hold true

$$\boldsymbol{C}_i = \boldsymbol{R}^T\ ({}^{I}\boldsymbol{C}_i), \tag{15}$$

$$\boldsymbol{\Omega}_i = \boldsymbol{R}^T\ \boldsymbol{\omega}_i. \tag{16}$$

The above two relations are used to map the hydrodynamic moment vectors and the angular velocity vectors between the inertial and rotating frames.

The equations governing the evolution of the quaternion parameters are given as follows (derivation can be found in Kuipers 1999),

$$\dot{\boldsymbol{q}} = \begin{bmatrix} \dot{q}_0 \\ \dot{q}_1 \\ \dot{q}_2 \\ \dot{q}_3 \end{bmatrix} = \frac{1}{2}\begin{bmatrix} 0 & -\Omega_{x_i} & -\Omega_{y_i} & -\Omega_{z_i} \\ \Omega_{x_i} & 0 & \Omega_{z_i} & -\Omega_{y_i} \\ \Omega_{y_i} & -\Omega_{z_i} & 0 & \Omega_{x_i} \\ \Omega_{z_i} & \Omega_{y_i} & -\Omega_{x_i} & 0 \end{bmatrix}\begin{bmatrix} q_0 \\ q_1 \\ q_2 \\ q_3 \end{bmatrix}. \tag{17}$$

Since we will be using a second-order scheme for updating the variables, equation (17) can be differentiated again to generate the second time derivative for $\boldsymbol{q}$.

The boundary conditions for the fluid velocity are:

$$\boldsymbol{u} = \boldsymbol{u}_b \text{ on } \partial\Gamma_u, \tag{18}$$

$$\boldsymbol{u} = \boldsymbol{U}_i + \boldsymbol{\omega}_i \times (\boldsymbol{x} - \boldsymbol{X}_i) \text{ on } \partial\Gamma_i, \tag{19}$$

where $\partial\Gamma_u$ is the boundary section where the fluid velocity, $\boldsymbol{u}_b$, is specified, and $\partial\Gamma_i$ is the surface of the ith particle. The boundary condition (19) can also be written as

$$\boldsymbol{u} = \boldsymbol{U}_i + (\boldsymbol{R}\boldsymbol{\Omega}_i) \times (\boldsymbol{x} - \boldsymbol{X}_i) \text{ on } \partial\Gamma_i, \tag{20}$$

where $\boldsymbol{R}$ is the rotation matrix as given in equation (14).

We solve the governing equations (1)–(3), and (12) to obtain the flow field and the particle velocities.

2.1. *Weak formulation*

In the fluid–particle systems, owing to the complex irregular nature of the domain occupied by the fluid, finite-element techniques are particularly powerful for discretizing the governing fluid equations. In order to use a finite-element method, we first seek a weak formulation that incorporates both the fluid and particle equations, namely equations (1)–(3) and (12).

Let us introduce the function space $\mathbb{V}$, given by

$$\mathbb{V} = \begin{cases} \boldsymbol{V} = (\boldsymbol{u}, \boldsymbol{U}_i, \boldsymbol{\Omega}_i) \,|\, \boldsymbol{u} \in H^1, (\boldsymbol{U}_i, \boldsymbol{\Omega}_i) \in \mathscr{R}^3 \\ \text{such that } \boldsymbol{u} = \boldsymbol{U}_i + (\boldsymbol{R}\boldsymbol{\Omega}_i) \times (\boldsymbol{x} - \boldsymbol{X}_i) \text{ on } \partial\Gamma_i \text{ and } \boldsymbol{u} = \boldsymbol{u}_b \text{ on } \partial\Gamma_u. \end{cases} \tag{21}$$

In the above, H^1 corresponds to the Hilbert space defined on the fluid domain, and $\mathscr{R}^3$ stands for the real space for the particle velocities. The space for the pressure is chosen as L^2 and is denoted by

$$\mathbb{P} = \{p \,|\, p \in L^2\}. \tag{22}$$

To derive the weak formulation for the combined fluid–solid system, we consider the variation of $\boldsymbol{V}$ (test function) given by

$$\tilde{\boldsymbol{V}} = (\tilde{\boldsymbol{u}}, \tilde{\boldsymbol{U}}_i, \tilde{\boldsymbol{\Omega}}_i) \in \mathbb{V}_0, \tag{23}$$

where the variational space $\mathbb{V}_0$ is the same as $\mathbb{V}$, except that $\boldsymbol{u} = 0$ on $\partial\Gamma_u$. Multiplying equation (2) by the test function for the fluid velocity, $\tilde{\boldsymbol{u}}$, and integrating over the fluid domain at time t, we have

$$\int_{\Gamma_0} \rho_f \left(\frac{\partial \boldsymbol{u}}{\partial t} + (\boldsymbol{u} \cdot \nabla)\boldsymbol{u} \right) \cdot \tilde{\boldsymbol{u}} \, \mathrm{d}V + \int_{\Gamma_0} \boldsymbol{\sigma} : \nabla \tilde{\boldsymbol{u}} \, \mathrm{d}V + \sum_{1 \leqslant i \leqslant N} \int_{\partial\Gamma_i} (\boldsymbol{\sigma} \cdot \hat{\boldsymbol{n}}) \cdot \tilde{\boldsymbol{u}} \, \mathrm{d}S = 0, \tag{24}$$

where Γ_0 is the domain occupied by the fluid. It should be noted that the variations for each variable introduced above are arbitrary except on the particle surface where the no-slip boundary condition equation (20) enforces the equality of variations of fluid and particle velocities given by the following relation

$$\tilde{\boldsymbol{u}} = \tilde{\boldsymbol{U}}_i + (\boldsymbol{R}\tilde{\boldsymbol{\Omega}}_i) \times (\boldsymbol{x} - \boldsymbol{X}_i). \tag{25}$$

Using (25) and the relations given by equations (3), (5), (8), (10)–(12), we can rewrite the surface integral inside the summation in equation (24) as follows

$$\int_{\partial\Gamma_i}(\boldsymbol{\sigma}\cdot\hat{\boldsymbol{n}})\cdot\tilde{\boldsymbol{u}}\,\mathrm{d}S=\tilde{\boldsymbol{U}}_i\cdot\int_{\partial\Gamma_i}(\boldsymbol{\sigma}\cdot\hat{\boldsymbol{n}})\,\mathrm{d}S+(\boldsymbol{R}\tilde{\boldsymbol{\Omega}}_i)\cdot\int_{\partial\Gamma_i}(\boldsymbol{x}-\boldsymbol{X}_i)\times(\boldsymbol{\sigma}\cdot\hat{\boldsymbol{n}})\,\mathrm{d}S$$
$$=\tilde{\boldsymbol{U}}_i\cdot\left[m_i\frac{\mathrm{d}\boldsymbol{U}_i}{\mathrm{d}t}-\boldsymbol{G}_i\right]+\tilde{\boldsymbol{\Omega}}_i\cdot\left[\boldsymbol{I}_i\frac{\mathrm{d}\boldsymbol{\Omega}_i}{\mathrm{d}t}+\boldsymbol{\Omega}_i\times(\boldsymbol{I}_i\boldsymbol{\Omega}_i)\right]. \tag{26}$$

Substituting equation (26) into equation (24) we obtain the combined fluid–particle momentum equation

$$\int_{\Gamma_0}\rho_f\left(\frac{\partial\boldsymbol{u}}{\partial t}+(\boldsymbol{u}\cdot\nabla)\boldsymbol{u}\right)\cdot\tilde{\boldsymbol{u}}\,\mathrm{d}V-\int_{\Gamma_0}p\nabla\cdot\tilde{\boldsymbol{u}}\,\mathrm{d}V+\int_{\Gamma_0}\mu\left[\nabla\boldsymbol{u}+(\nabla\boldsymbol{u})^T\right]:\nabla\tilde{\boldsymbol{u}}\,\mathrm{d}V$$
$$+\sum_{1\leqslant i\leqslant N}\tilde{\boldsymbol{U}}_i\cdot\left[m_i\frac{\mathrm{d}\boldsymbol{U}_i}{\mathrm{d}t}-\boldsymbol{G}_i\right]+\sum_{1\leqslant i\leqslant N}\tilde{\boldsymbol{\Omega}}_i\cdot\left[\boldsymbol{I}_i\frac{\mathrm{d}\boldsymbol{\Omega}_i}{\mathrm{d}t}+\boldsymbol{\Omega}_i\times\boldsymbol{I}_i\boldsymbol{\Omega}_i\right]=0. \tag{27}$$

The weak formulation for the mass conservation equation is obtained in a similar way to that outlined above. Let $\tilde{p}$ be the variation of pressure p such that $\tilde{p}\in\mathbb{P}$. Here, the function space for both $\tilde{p}$ and p are chosen to be the same since there are no explicit boundary conditions for the pressure. The weak form of equation (1) is then given by

$$\int_{\Gamma_0}\tilde{p}(\nabla\cdot\boldsymbol{u})\,\mathrm{d}V=0. \tag{28}$$

The details of ALE formulation, spatial and temporal discretization, mesh generation, and schemes for projecting the variables from the old to the new mesh can be found in Hu *et al.* (2001).

3. Validation

To validate our numerical code, tests of an ellipsoid freely moving in Poiseuille flows were performed and the results were compared with those of Sugihara-Seki (1996) under Stokes flow conditions. The conditions therein were reproduced with one difference. Sugihara-Seki assumes the particles to be massless (and thus inertialess), and so no net force or torque acts on the particle. However, in this work, even though the density of the particles can be made quite small (the Stokes number, which characterizes the particle inertia, is of order 10^{-6}), it cannot be put identical to zero. Consequently, there exists a certain force and torque, albeit small, that acts on the particle and tends to produce translational and angular accelerations. This acceleration thus leads to a small transient period. The inertial terms in the Navier–Stokes equation are put to zero in the comparison tests.

Sugihara-Seki (1996) presented (in his figure 4) the variation of translational and angular velocity of an ellipsoid, suspended in a Poiseuille flow within a tube of radius 1.0, as a function of its orientation angle inside the tube at different locations. These velocities have been computed here and compared, as shown in figure 1. In the plots, the ellipsoid with its major axis $a=0.8$ and minor axes $b=c=0.2$ is initially located at the radial position $Y=0.15$, and its orientation angle θ is varied. The notation and normalization used there (normalization of the velocity is with the maximum velocity at the inlet and normalization of the angular velocity is with the ratio of the maximum velocity at the inlet to the tube radius), have been followed for presenting the results in this section. It is seen that the results agree very well (within 1 %). The particle trajectories presented in figure 7 of Sugihara-Seki (1996) also match those computed in this study.

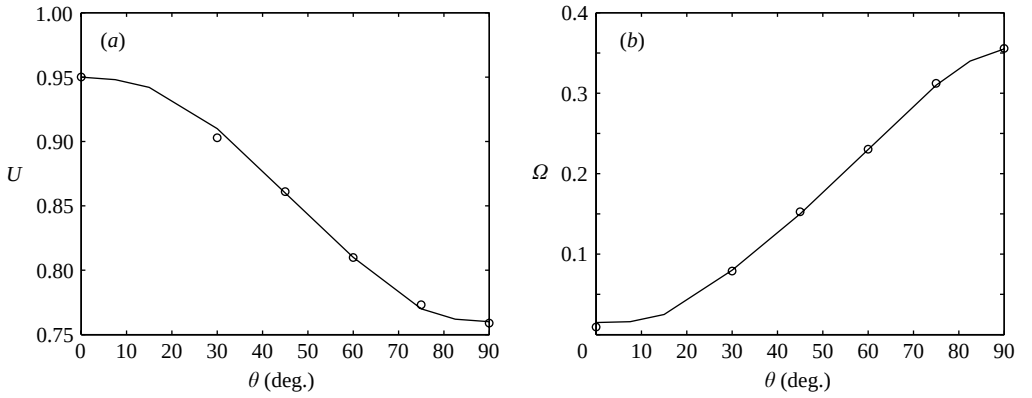

FIGURE 1. Comparisons of the values of velocities of a spheroid in a Poiseuille flow under Stokes flow conditions. The spheroid is initially placed at an off-centre location with various orientations. The line indicates data in figure 4 of Sugihara-Seki (1996) while the dots represent values obtained in this study. (*a*) Translational velocity of ellipsoid. (*b*) Angular velocity of ellipsoid.

Sedimenting ellipsoids, simulated using this numerical scheme, also follow the well-known property of turning their broadside orthogonal to the direction the flow for the case of non-zero Reynolds numbers (Cox 1965), and of moving in a direction between the directions of the gravity and the orientation of the long axis for Stokes flow (Jeffery 1922). The rocking motion of a settling ellipsoid at higher Reynolds numbers (Pan *et al.* 2003) is also observed.

4. Set-up

The problem set-up consists of an axisymmetric ellipsoid (prolate spheroid) of aspect ratio (the ratio of the long to the short axis) 2:1, settling in a circular tube of diameter D, with the centre of the ellipsoid initially located on the axis of the tube. The gravity is acting along the axis of the tube as indicated in figure 2. The major and minor axes of the ellipsoid are $a = D/8$ and $b = c = D/16$, respectively. To simulate the motion of the ellipsoid in an infinitely long tube, the computational domain moves with the ellipsoid. The two ends of the computational domain are kept at a distance of $40a$ from the centre of the ellipsoid on both sides at all times such that as the ellipsoid moves, any end-effects are minimized. The inlet boundary has a zero velocity condition (no flux at the bottom end), while the outlet boundary has a no-stress condition (outflow condition at the top end). For an understanding of this technique see Hu *et al.* (1992) and the description therein. Numerical experiments were performed by us to determine the length of tube necessary to ensure that the end-effects do not play a role in the motion of the body. This was done by moving the two ends away from the centre of the spheroid in increments and observing the spheroid's motion (its velocity and path). After the ends are at a distance of $40a$, there is no further change in the dynamics of the body, and thus this distance is sufficient to ensure that the motion is unaffected by these two boundary locations. This length is thus determined as the physical length of tube required to simulate the dynamics in an infinitely long tube. The orientation of the ellipsoid can be described by the angle between the line containing the major axis of the ellipsoid and the direction of gravity, represented by β ($-90^\circ < \beta < 90^\circ$), as shown in figure 2. A view of the

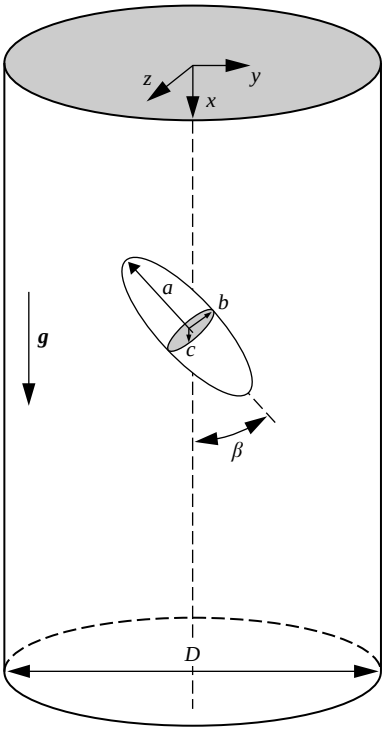

FIGURE 2. Geometry of an ellipsoid initially oriented at an angle β and located at the centre of a cylindrical tube. D is the tube diameter, a, b, c are the major and minor axes, respectively. The focus in this study is on a spheroid ($b = c$).

finite-element mesh used in the simulations is shown in figure 3. Mesh convergence tests, similar to that performed to determine the length of tube required to simulate behaviour in an infinitely long tube, indicate that this mesh is fine enough to resolve the flow field for the Reynolds numbers presented in this study.

Starting at time $t = 0$, the spheroid is released from its initial position and is allowed to settle freely inside the tube. The motion of this spheroid is tracked. The simulation is carried out until a steady state is reached if one exists, or until a definite conclusion about the particle's trajectory can be drawn. The results from the various test cases have been presented in the next section.

5. Results and discussion

The parameters defining this problem are the flow Reynolds number based on the particle characteristic settling velocity and the long axis of the ellipsoid (Re), the ratio of densities of the particle to that of the fluid (ρ_p/ρ_f), and the initial orientation of the particle with respect to the direction of gravity (which is also the direction of the axis of the cylinder), as described by the angle β in figure 2. The effect of the aspect ratio of the particle (a/b) has also been explored. The rest of the parameters such as the initial radial location of the particle and the relative size of the particle with respect to the tube diameter are fixed in this study.

It can be seen from the symmetry consideration, that in the given set-up, there exist two orientations of the ellipsoid, which represent equilibrium configurations when the centre of the ellipsoid lies along the axis of the tube. These orientations

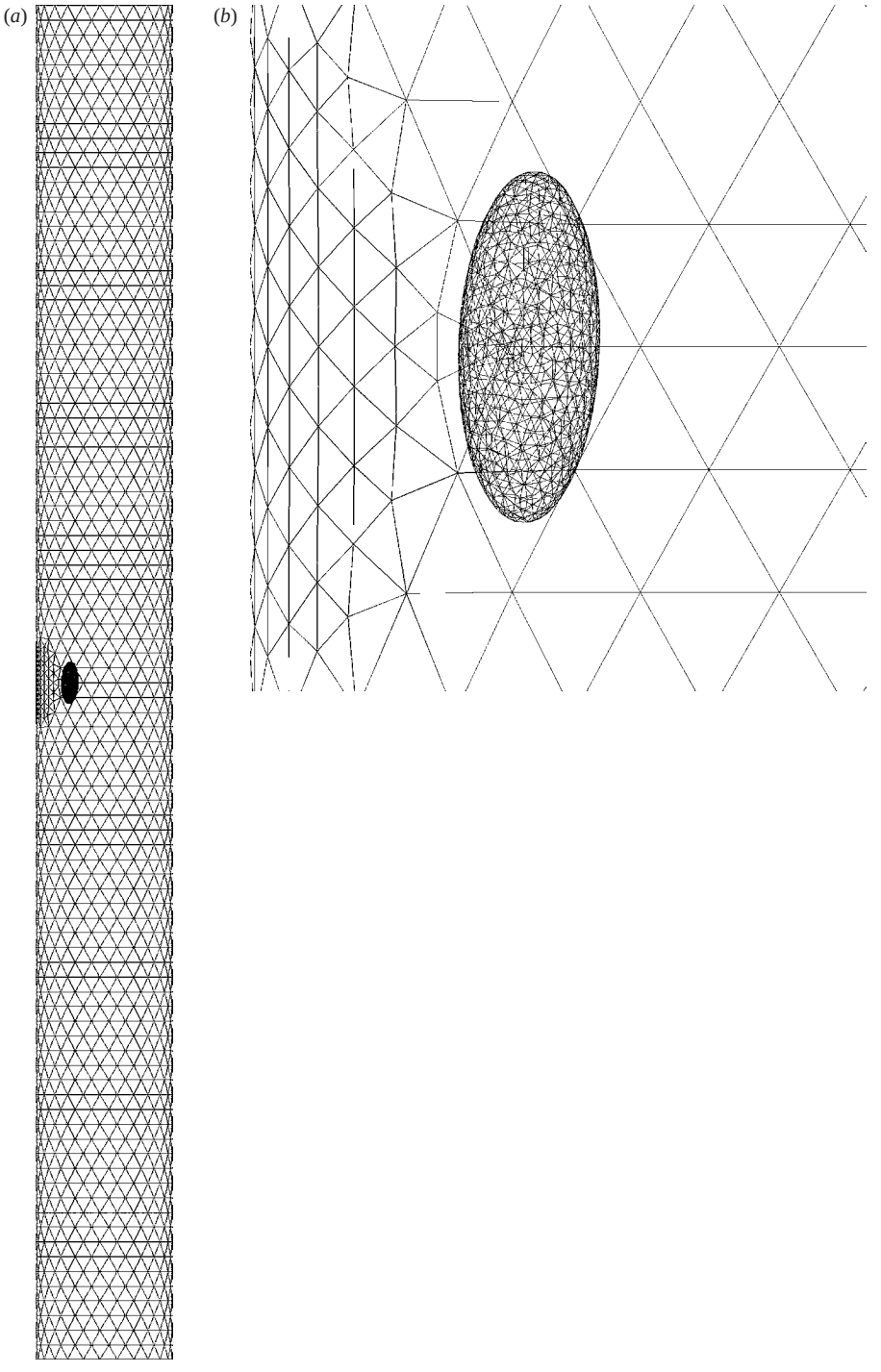

FIGURE 3. Finite-element mesh for a spheroid settling in a circular tube. (*a*) Overall view of the computational domain. (*b*) Surface meshes on the spheroid and the region on the cylindrical tube where the spheroid is the closest. The mesh consists of 35 891 quadratic tetrahedral volume elements, 6864 surface nodes and 51 286 total nodes in the volume.

are given by the configuration when the long axis of the ellipsoid is either aligned with the tube axis ($\beta = 0°$), or is perpendicular to it ($\beta = 90°$). For the motion in an infinite Newtonian fluid, at a non-zero Reynolds number, the orientation with the axis perpendicular to the direction of gravity ($\beta = 90°$) is known to be stable while the other orientation(s) is(are) unstable (Cox 1965). This result is not valid when the Reynolds number is high enough to cause inherent unsteadiness due to vortex shedding. The onset of unsteadiness at a critical Reynolds number will be a subject of future investigations. Under Stokes flow conditions in an infinite medium, an ellipsoid settles steadily along a direction between the gravity and its orientation and does not rotate (Jeffery 1922). However, the bounding walls of the tube, in which the ellipsoid is settling, may induce forces and torques, such as those shown in Happel & Brenner (1980, pp. 298–321), which change the motion of the ellipsoid. The forces and torques on a sphere moving along the axial direction in a circular tube have been evaluated in that study using a method of reflections.

5.1. *Motion of a spheroid without inertia in Stokes flow*

The inertial terms in the fluid momentum equation (2), can be set identical to zero in the numerical calculations, which leads to a linear set of equations, the Stokes equations. The first objective in this study is to investigate the motion of an ellipsoid in a bounded domain, under Stokes flow conditions, and to determine how the particle inertia affects this motion. For an inertialess particle, the value of the dimensionless parameter (Stokes number) $\rho_p v_p a/\mu$ is selected to be very small (of the order of 10^{-5}), where v_p is the characteristic settling velocity of the ellipsoid.

It is well known that the expected motion of an inertialess particle in Stokes flow, has to be time reversible. This implies that if the direction of the external force (here gravity) is reversed, the particle should retrace the path travelled by it. It is also known that under Stokes flow conditions and in an infinite medium, a non-spherical body (for example an ellipsoid) settles steadily, and the motion of the body is along a direction between the direction of gravity and the direction given by the long axis of the body (Cox 1965). When the ellipsoid is confined inside a tube, if the particle is oriented symmetrically, ($\beta = 0$, $\beta = \pi/2$ etc.), it does not experience any lateral force since it does not have any preferred direction of motion. However, for all other orientations, the ellipsoid moves towards the tube wall and thus the dynamics of its motion depends on the nature of the wall–particle interaction that inevitably occurs.

In the current set-up, owing to symmetry considerations, the spheroid should only move in the (x, y)-plane and rotate about the z-axis (figure 2). In view of this, we constrain the simulation such that the spheroid is restricted to a translation in the (x, y)-plane and a rotation about the z-axis. If such a constraint is not applied, numerical errors accumulated over time may eventually break the symmetry. The motion of a completely free spheroid has been discussed in a subsequent section.

The motion of an inertialess spheroid, initially centred, sedimenting in an infinitely long tube is depicted by a sequence of snapshots taken at regular time intervals in figure 4 with the particle centred vertically in each shot.

The initial motion of the particle, when it is released from rest at the centre of the tube, is relatively unaffected by the presence of the tube wall. As the spheroid settles, it moves towards the wall, as seen in figure 4(a–c). In studying the motion of a spheroid moving between stationary walls in Happel & Brenner (1980, pp. 332–337), it has been observed that the spheroid rotates owing to the torque exerted by the flow field. The direction of this torque is seen to be a function of the spheroid's aspect ratio. In a similar fashion, in figure 4(c–e) it can be seen that as the spheroid approaches the

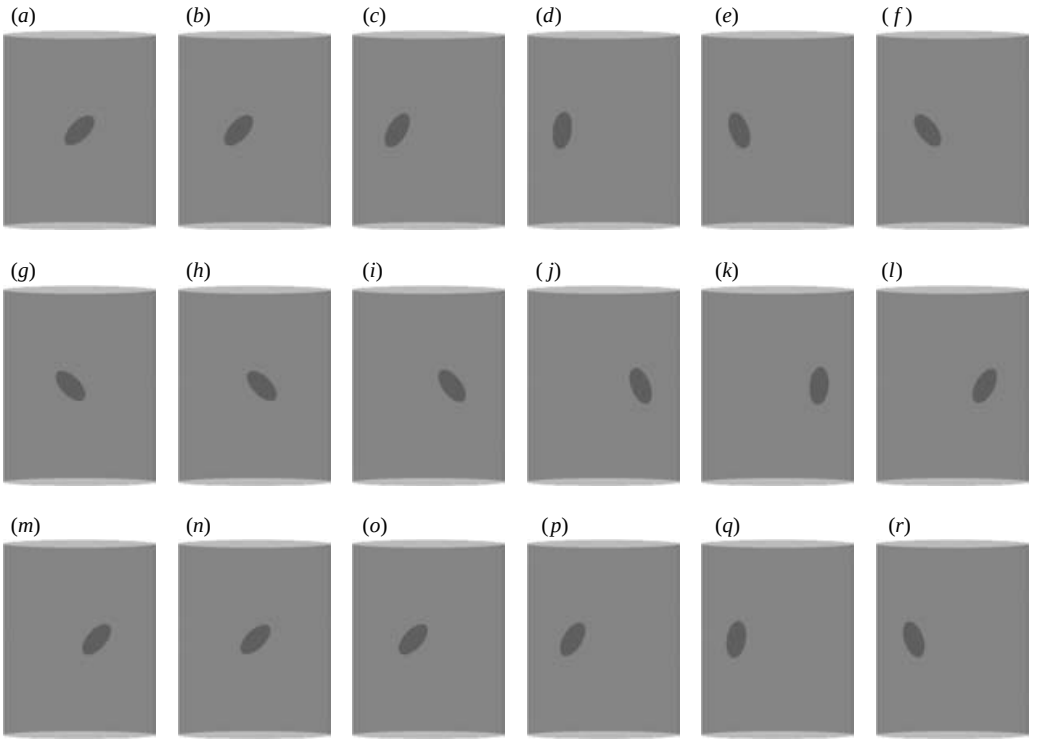

FIGURE 4. Sedimentation of an inertialess spheroid inside a tube under Stokes flow conditions. The initial angle of orientation is $\beta = -45^{\circ}$, and the aspect ratio of the spheroid is $a/b = 2.0$. The tube diameter is D is $8a$. One period of oscillation will be comprised of panels from (a) to (n). The corresponding distance travelled along the length of the tube is shown in figure 5. The time elapsed between consecutive panels is constant.

sidewall of the tube, it experiences a torque which rotates the particle. The direction and magnitude of this torque will be a function of the aspect ratio and the angle of approach of the spheroid, and the tube radius. In the present set-up (initial orientation $\beta = -45^{\circ}$, $a/b = 2$), the direction of rotation is first counterclockwise. The spheroid rotates near the wall such that its new orientation, after undergoing the rotation, is exactly opposite (i.e. given by a new direction of $-\beta$) to the one at which it was oriented while approaching the wall, which is seen in figure 4(e–g). Thus, its lateral motion is now in the direction opposite to the one at which it initially started, with its orientation reversed, shown in figure 4(g–j). Subsequently, because of the periodic reversal of orientation of the particle, a periodic side-to-side motion is set up with the particle moving towards one side of the cylinder wall, rotating near it, reversing its direction of motion and then moving towards the other side. Such a periodic motion was also observed by Liu *et al.* (2004) in their experiment of a cylinder falling in a long tube. The period of oscillation from one side to the other, naturally, is a function of the initial orientation and the radius of the tube in which the spheroid is falling. As the initial orientation of the spheroid becomes more vertical, the period of its oscillatory motion is seen to increase. A decrease in the period is seen with a decrease in the radius of the tube. It can be seen that such a motion also satisfies the time reversibility expected from such a system. The motion of the centre of the spheroid follows the path shown in figure 5.

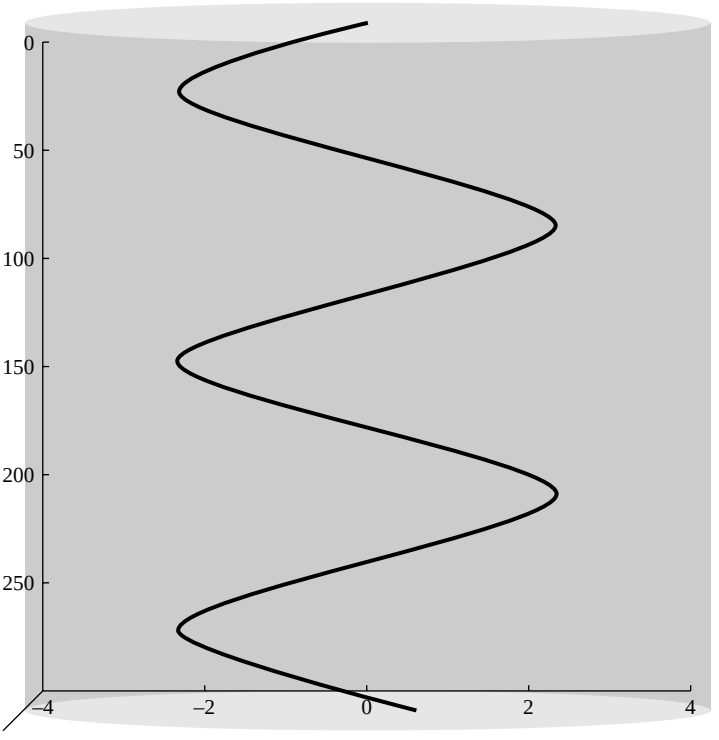

FIGURE 5. Motion of the centre of an inertialess spheroid, settling inside a tube under Stokes flow conditions. The motion occurs in the (x, y)-plane. The initial angle of orientation is $\beta = -45^\circ$. The amplitude of this oscillation is 2.24 (corresponding to a dimensionless value of 0.56).

In summary, an inertialess spheroid follows a perfectly periodic orbit when settling in a long tube under Stokes flow conditions. The motion shown in figure 4 is consistent with the observed 'glancing' motion in Russel *et al.* (1977) for a rod between two parallel plates. Figure 6 shows the amplitude of this periodic motion as a function of the initial orientation of the spheroid, β, as defined in figure 2. The amplitude has been normalized with the tube radius $D/2$.

The increase in the amplitude of the oscillatory motion with an increase in the orientation β can be explained on the basis of how the direction of motion of the spheroid varies with its orientation. In the absence of external torques (as in Stokes flow in an infinite medium), this direction is between the direction of gravity and the direction of orientation of the long axis (Cox 1965), (say ϕ, $0 < \phi < \beta$). Thus with an increase in β, the angle of motion ϕ also increases. The spheroid continues to move in this direction towards the wall until the torque induced by the wall rotates it to the vertical orientation ($\beta = 0^\circ$) after which it starts to move away from the wall, as seen in figure 4. Hence, the larger the initial angle of orientation, the longer the time required to rotate the particle back to $\beta = 0^\circ$, and hence, the longer it will continue to move towards the wall.

It can be imagined from figure 2, that the maximum amplitude of oscillation that can be achieved is given by $D/2 - b$ which when normalized with the tube radius gives a value of 0.875 for the present set-up. Upon examining the trend in figure 6, it can be seen that there will exist a particular value of initial orientation at which

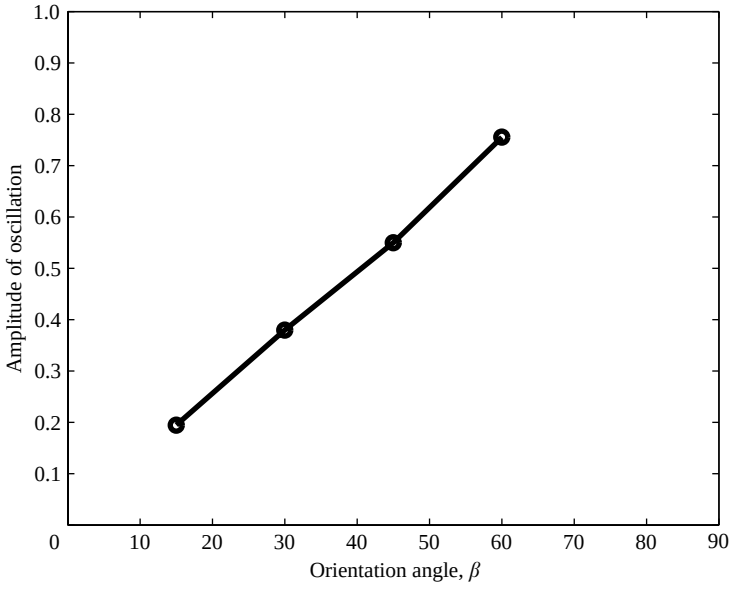

FIGURE 6. Amplitude of the oscillation (normalized with the tube diameter) of a spheroid in a tube as a function of its initial orientation. The tube diameter is kept fixed at $D = 8a$ and the aspect ratio of the spheroid is $a/b = 2$.

this amplitude will be reached. Through numerical experiments, it is found that this corresponds to an initial orientation of around 70°. At this critical orientation angle, the spheroid moves to a location near the wall wherein the smallest gap between the particle and the tube wall is so small (less than 0.1 % of the short axis of the spheroid) that it essentially can be considered as a collision between the spheroid and the cylindrical wall. Naturally, it follows that since the amplitude increases with initial β, collision occurs for all orientations higher than the critical value $\beta > 70°$. Furthermore, the critical angle beyond which collision occurs, is a function of the aspect ratio of the spheroid. To understand the reason for this collision, figure 7 shows the variation of the torque with the radial position for a spheroid, constrained to settle vertically without rotation, in a tube under Stokes flow conditions. The value of the torque has been normalized with $Vag(\rho_p - \rho_f)$, where V is the volume of the spheroid, a is the length of the major axis, and g is the acceleration due to gravity. The radial position has been normalized with the tube radius $D/2$.

The direction of torque acting on the spheroid, changes at a particular radial location. In figure 4(*h–m*), it was seen that the rotation of the spheroid, was about the negative z-axis. This direction of rotation can be characterized as reverse-contact, i.e. the particle rotates as if it is rolling up the tube near the closest contact (Liu *et al.* 1993). If the particle is restrained from this rotation, the resultant torque acting on it can be called a 'reverse-contact torque'. This reverse-contact torque is responsible for eventually moving the spheroid away from the wall, as in figure 4(*m–p*). However, as the spheroid comes closer to the wall, the torque changes direction. The reverse-contact torque decreases the angle of orientation β, when $0° < \beta < 45°$, which in turn reduces the lateral force taking the spheroid towards the wall. A reversal of torque will have the opposite effect and thus will take the spheroid closer to the tube wall. Figure 7 also shows that as the orientation angle β is increased, the magnitude of reverse-contact torque reduces, i.e. the reverse-contact rolling of the particle, which

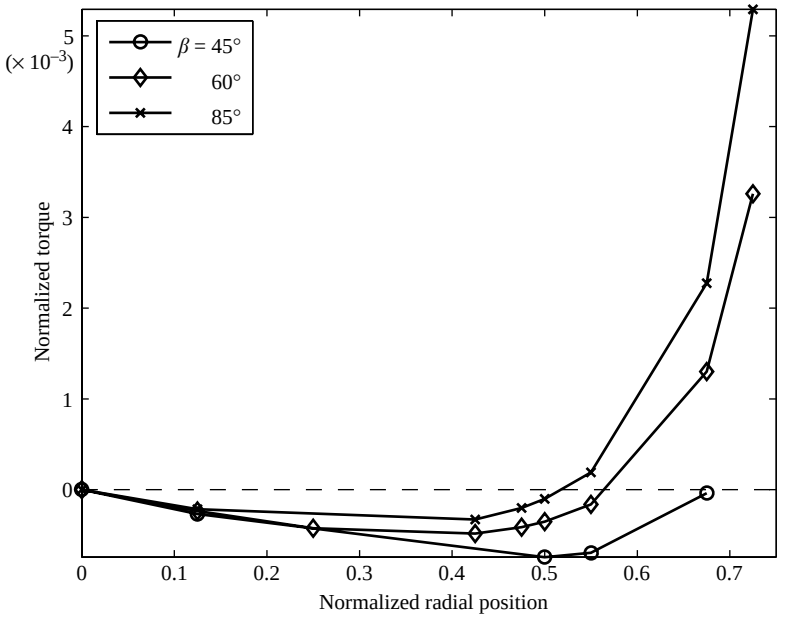

FIGURE 7. Normalized torque acting on a spheroid as a function of its normalized radial position in the tube. The spheroid is on the right-hand side of the tube, similar to those seen in figure 4(*h–j*). The torque has been normalized with $Vag(\rho_p - \rho_f)$ and the radial position has been normalized with the tube radius.

counteracts the motion towards the wall, is reduced. Consequently, an increase in the orientation angle β causes an increase in the amplitude of oscillation, and eventually a collision.

The aspect ratio, e, of a spheroid is defined as the ratio of the long to short axis ($e = a/b$ from figure 2). Thus, a spheroid with an aspect ratio of value one is a sphere. As the value of e changes, the period of motion from one side to the other and the amplitude of this oscillation change accordingly. This variation is shown in figure 8. The amplitude has been normalized with the tube radius $D/2$.

A sphere will fall vertically if it is released from the centre of the tube, corresponding to a motion with zero amplitude. The lateral force acting on a spheroid increases as its aspect ratio is increased (Jeffery 1922), which carries the particle closer to the tube wall as seen. At a large enough value of e, collision with the wall may occur. The combined effect of the aspect ratio and the angle of orientation, determines the periodic motion of a spheroid settling in an infinite tube in Stokes flow.

5.2. *Motion of a spheroid with inertia in Stokes flow*

The motion of a spheroid with inertia in a Stokes flow can follow different dynamics from the one outlined above, as demonstrated in Broday *et al.* (1998) for spheroids in shear flows. The effects of particle inertia can be characterized by the particle Stokes number $St = \rho_p v_p a/\mu$, where ρ_p is the density of the particle, v_p is the characteristic velocity of the particle, a is its characteristic size (long axis of the spheroid), and μ is the viscosity of the suspending fluid. This Stokes number can also be understood as being proportional to the ratio of the viscous relaxation time of a particle $t_p = m/6\pi\mu a$ to the flow time a/v_p, where m is the mass of the particle. The ratio of the Stokes number to the Reynolds number, is the density ratio ρ_p/ρ_f. In a numerical approach, we can investigate independently the effects of particle inertia and fluid inertia on the

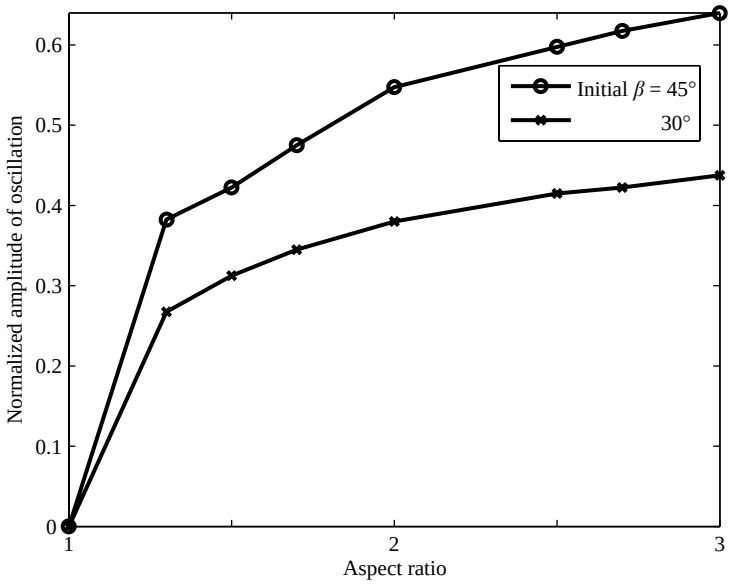

FIGURE 8. Normalized amplitude of oscillation of a spheroid in a tube as a function of its aspect ratio. The plots for two initial values of the orientation $\beta = 30°$ and $45°$ are presented. The amplitude has been normalized with the tube radius.

particle motion. The decoupling of these two allows us to understand the underlying physics better. The inertial terms in the governing fluid equations are set to zero and the resulting system is called Stokes flow with zero Reynolds number. The same is not done for the Stokes number.

A spheroid in an infinite medium under Stokes flow conditions does not experience any torque. However, near a wall, the particle does experience a torque which gives rise to an angular acceleration and velocity. Herein comes a difference in the spheroid's motion as compared to the case of an inertialess spheroid. It was shown earlier, that the orientation of an inertialess spheroid is perfectly periodic during its sedimentation (see figure 5). Figure 9 demonstrates that the motion (both position and orientation) of a spheroid with inertia is oscillatory, but not perfectly periodic. The amplitude of this side-to-side oscillatory motion is seen to increase over time.

As shown in figure 9, a spheroid with inertia settling in Stokes flow, experiences an increase in its orientation, whereby over periods of oscillations, it tends to migrate towards a configuration in which its long axis is perpendicular to gravity. The change in the spheroid's orientation over periods of oscillatory motion is shown in figure 10. This rate of change of the orientation angle is found to be a function of the Stokes number. It is observed that the spheroid eventually approaches a critical orientation angle at which the spheroid collides with the sidewall of the tube. Particles with higher Stokes numbers tend to reach this orientation faster (within fewer periods). The effect of the Stokes number on the rate of change of the orientation is shown in figure 11. The change is measured for a spheroid, initially oriented at an angle of $\beta = 45°$, over the first few cycles of its motion, which is equal to the initial slope of the curve in figure 10. However, it can be seen from the slopes of the curves in figure 10 that this rate of change is nearly independent of the initial angle of orientation, and levels off after a certain number of cycles have elapsed.

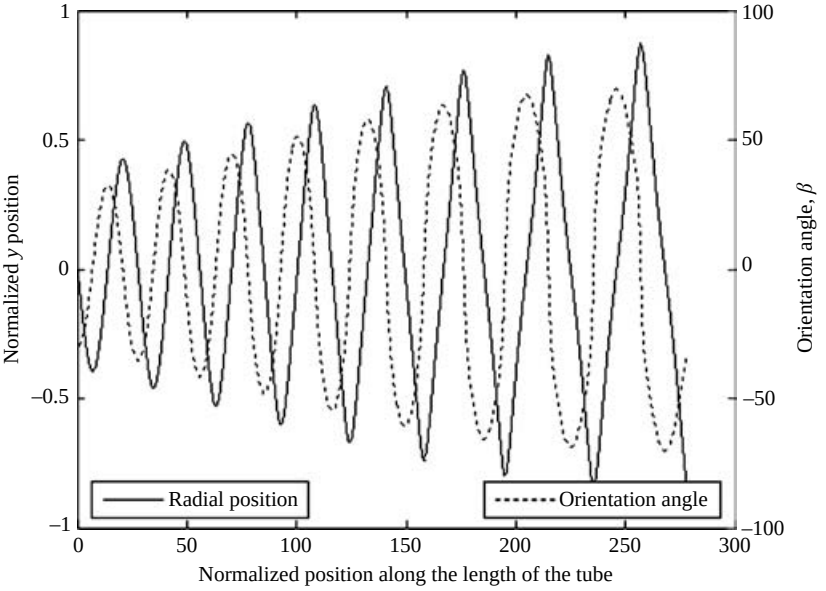

FIGURE 9. Motion of a spheroid with inertia settling inside a tube under Stokes flow conditions. The spheroid moves in the (x, y)-plane and rotates about the z-axis. The initial orientation of the spheroid is -30° and the mean Stokes number is around 22.5. The tube diameter is $D = 8a$ and the aspect ratio of the spheroid is $a/b = 2$. The normalization has been done with the tube radius. The orientation angle is measured in degrees.

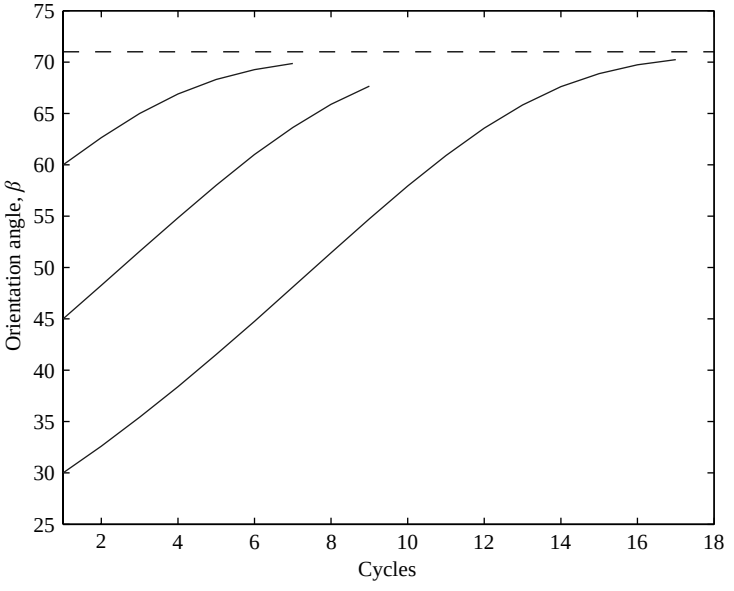

FIGURE 10. Change in the orientation of a spheroid with inertia, as it falls in a long tube. The orientation angle (in degrees) is measured when the centre of the spheroid coincides with the axis of the tube. The dotted line indicates the critical orientation angle at which the spheroid collides with the sidewall of the tube. The mean Stokes number is around 22.5.

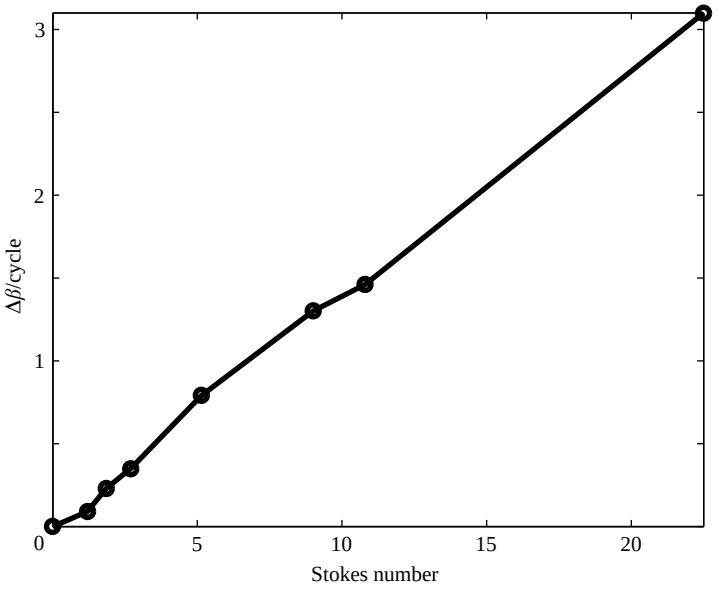

FIGURE 11. Change in the orientation angle per cycle as a function of the particle Stokes number. The change is measured in degrees.

The increase of the orientation angle over each cycle, as the spheroid rotates near the wall, is certainly due to the particle inertia. For a spheroid without inertia, the net torque and force acting on it are always zero and so are the angular and translational accelerations. Thus, the particle's translational and angular velocities respond instantaneously to a change in the flow around the particle. However, for a spheroid with inertia, a torque opposing its rotation causes a deceleration which takes a finite time to change its angular velocity. This causes the angular velocity of the particle to lag behind the changes in the local flow field. An effect of this lag is that the spheroid rotates more (over-rotates), causing further increase in its maximum orientation. The effect of increasing inertia, as seen by the increase in the Stokes number in figure 11, is to further increase this effect and hence the faster change in the particle orientation. A consequence of this increase in the orientation over time is the increase of the amplitude of the spheroid's trajectory as it moves from side to side. This increase is illustrated in figure 9 and can be explained by combining the inertia effect with the effect due to the change of orientation seen in figure 6.

Figure 10 shows that the orientation angle approaches a limiting value of around 70°, irrespective of its starting value, after a few oscillations. In figure 6, it was seen that at this angle, the spheroid collides with the sidewall of the tube. In simulations, when the spheroid becomes close to the tube wall, finer meshes are introduced in the gap between the spheroid and wall to resolve the flow field there. These simulations capture the exact hydrodynamic forces acting on the spheroid. The minimum gap in a case for an inertialess particle with an initial orientation angle of $\beta = 75^\circ$ is shown in figure 12. It is seen that this number drops monotonically to a very small value (0.1 % of the particle diameter). Since the local mesh size is comparable to this gap size, the number of elements in the region goes up as this gap reduces, thereby increasing the size of the numerical simulation. Furthermore, a reduction in the time step is required to resolve this collision process. These two factors make the full spatial and temporal resolution of the collision process prohibitively expensive. This monotonic drop of

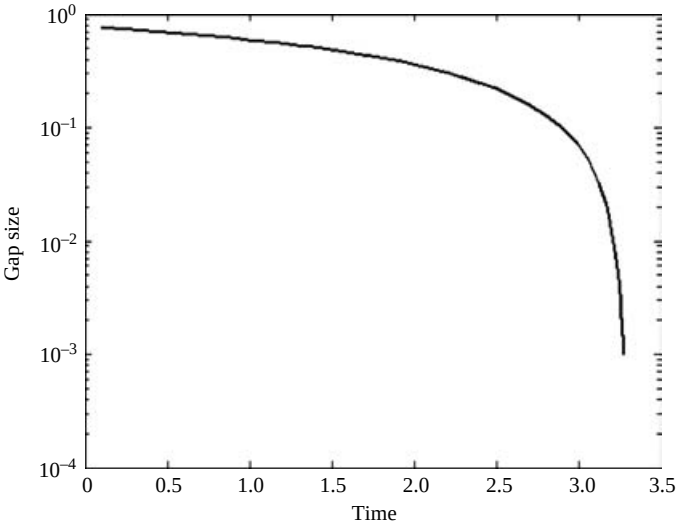

FIGURE 12. Minimum gap between a spheroid and the cylinder wall as a function of time. The ellipsoid was released from an initial angle of $\beta = 75^\circ$. The tube diameter is $D = 8a$ and the aspect ratio of the spheroid is $a/b = 2$. The mean Stokes number is around 22.5. The normalization of the gap has been done with the tube radius. The normalization of time has been done with $4\rho_f a^2/\mu$.

the minimum gap size, also indicates that actual collision occurs between the particle and the wall. In such cases, capturing collision without modelling film rupture is not possible. Similar collision, between a rod and a planar wall, was predicted using lubrication theory by Russel *et al.* (1977).

To circumvent this difficulty, a simple collision model was developed where short-range contact forces normal to the surface of the spheroid are used to prevent the spheroid from touching the wall. This model is activated when the minimum gap between the spheroid and the boundary wall is less than 5 % of the long axis of the spheroid a. This collision model acts to provide an inelastic collision between the two objects. It acts at the point of impact of the two surfaces and the collision force is normal to the colliding surface at this point. The value of the collision force is controlled so that the body is pushed away from the collision point and the new minimum distance between these two surfaces is 5 % of the long axis of the spheroid. In simulations where frequent collisions were not seen, no collision model was used and the hydrodynamics in the gap, manifesting itself as a lubrication force, naturally prevents overlap of the two surfaces.

A spheroid at a finite Stokes number, when released from an initial orientation angle less than the critical angle, tends to approach an orientation close to the critical angle and thus collides with the tube wall. For the initial orientations less than 70°, it was seen, as in figure 4, that the rotation of the spheroid near the wall always reverses its orientation (reverse-contact rolling along the closest wall). However, for the initial orientations larger than 70°, the direction of rotation is in the sense that the spheroid rotates through the horizontal orientation, $\beta = 90^\circ$, at the contact in collision (with regular rolling around the contact point). This is shown in figure 13. These two types of motion, reverse-contact and regular rolling, can be compared to the 'glancing' and 'reversing' motion analysed by Russel *et al.* (1977).

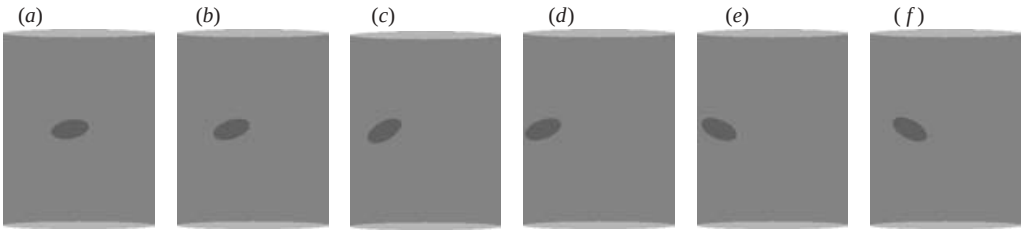

FIGURE 13. Motion of a sedimenting spheroid near the sidewall, at orientations exceeding the critical value. The initial orientation of the spheroid is 105° and the mean Stokes number is around 22.5. The tube diameter is $D = 8a$ and the aspect ratio of the spheroid is $a/b = 2$.

Using the simple collision model, it was seen that a spheroid with inertia, after colliding with the sidewall, eventually settles into a perfectly periodic orbit, as shown in figure 14. Consider the motion of the spheroid in one period of oscillation as presented in figure 14(*b*). The particle moves left across the centreline of the tube with an orientation of around 105° (equivalent to −75°). While the particle is approaching the wall, it experiences a reverse-contact torque (see figure 7) which rotates the spheroid towards a more vertical orientation. When the particle becomes very close to the wall, it collides with the tube wall at an orientation of around 125° (or −55°); its settling velocity decreases sharply and it rotates in a direction opposite to the reverse-contact sense, which gives rise to the sharp transition in the orientation angle. Once the particle rotates across the horizontal orientation, $\beta = 90°$, it starts to move away from the wall. The direction of torque once again becomes reverse-contact after the spheroid has moved a certain distance from the wall. This torque is responsible for the local peak as the particle crosses the centreline towards the right-hand side because it acts in opposite directions on the two sides of this centreline. This oscillatory motion is a stable limit cycle, and unlike the case shown in figure 5, contains both reverse-contact and regular rolling.

It can be seen that the only torque on the spheroid is due to the sidewall since in an infinite medium there is no torque. The only position with net zero wall torque is when the centre of the spheroid is exactly on the axis of the tube and the spheroid is oriented at an angle of either 0° or 90°. Hence, these are the only two possible equilibrium orientations. However, because of the reasons stated previously, neither of these is stable. Over many cycles, the orientation of a spheroid with a finite Stokes number, is seen to approach a value close to the critical value. Thus, an initial orientation of $\beta = 0°$ and $\beta = 90°$ can be classified as 'unstable' orientations and there is a limit cycle near the critical orientation angle. In the case of zero Stokes number, these two orientations are 'centres' with the existence of periodic orbits near them. Thus, the non-reversibility introduced by the particle inertia manifests itself by altering the characteristics of the equilibrium configurations.

5.3. *Motion of an unconstrained spheroid in Stokes flow*

As discussed above, if a spheroid is released at the centre of a long tube, owing to symmetry considerations, its motion will be confined to a plane containing the long axis of the spheroid and the axis of the tube. However, in numerical simulations, because of the asymmetry in the finite-element mesh, small errors in the hydrodynamic forces and torques will perturb the motion of the spheroid and push it away from the symmetry plane. Since there is no hydrodynamic force to restore the particle to its original symmetry plane, the particle will generally wander in the tube as it

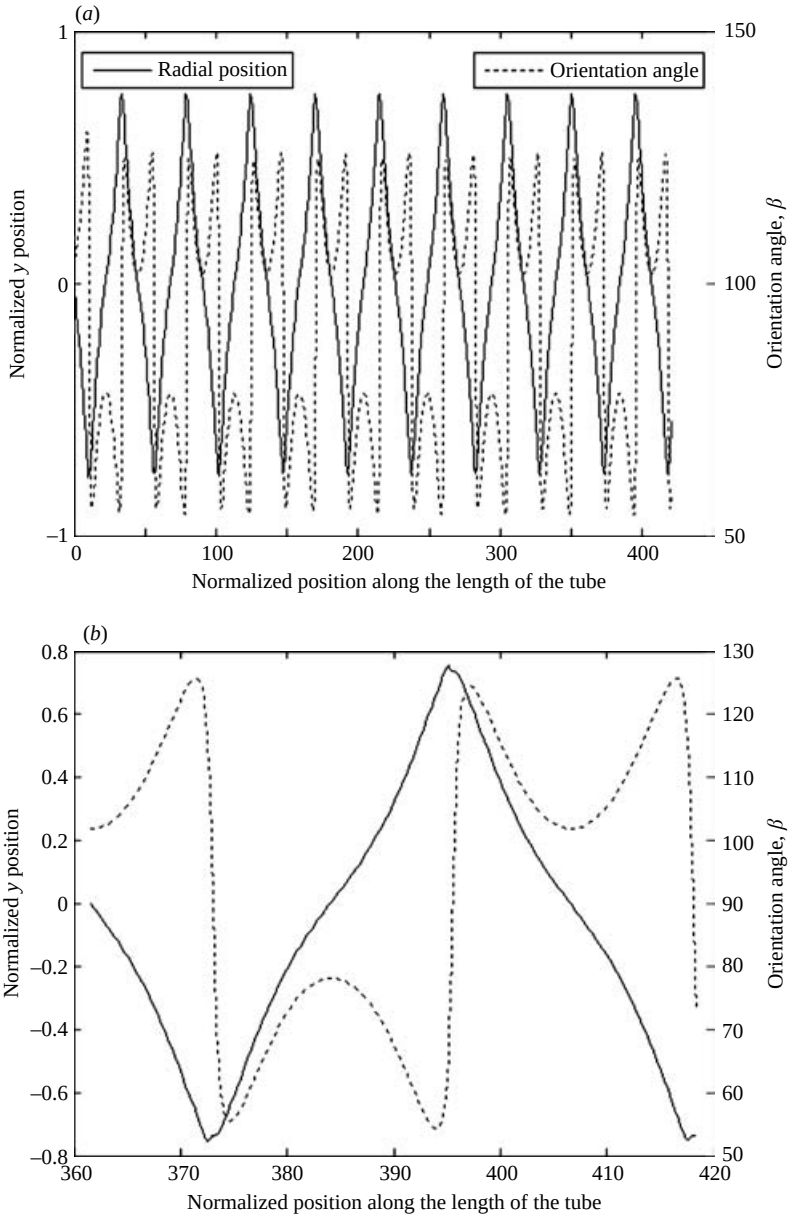

FIGURE 14. Long-term periodic motion of a spheroid with inertia settling inside a tube under Stokes flow conditions, after it collides with the tube wall. The initial orientation of the spheroid is 105° and the mean Stokes number is around 22.5. The normalization has been done with the tube radius. Snapshots of the particle position are presented in figure 13. (*a*) Motion over many periods. (*b*) Zoom in view of the motion over one period.

settles. To prevent the buildup of these errors over time, in the simulations presented so far, these erroneous forces have been set to zero, and thus the motion of the body is somewhat constrained. In any practical system, these errors can be associated with imperfections of experiments such as surface roughness, disturbances caused by external factors, etc. Figure 15 shows an example of a three-dimensional motion of

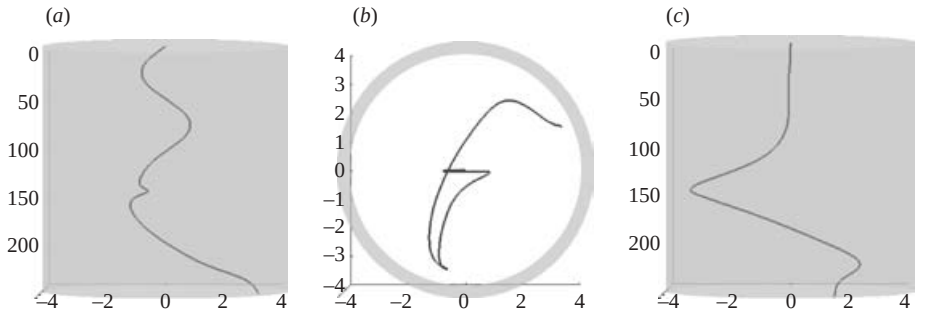

FIGURE 15. Path of the centre of an unconstrained inertialess spheroid falling in a tube under Stokes flow conditions. Initial orientation of the spheroid is $\beta = -15^\circ$. The aspect ratio of the spheroid is $a/b = 2.0$ and the tube diameter is $D = 8a$. (*a*) (x, y)-view. (*b*) (y, z)-view. (*c*) (x, z)-view.

a completely unconstrained spheroid wherein these erroneous forces act and displace the motion of the spheroid from its symmetry plane.

In figure 15, an inertialess spheroid was released from the centre, with its initial orientation $\beta = -15^\circ$ and was allowed to settle freely. Initially, its motion is similar to that of a constrained spheroid. However, after the particle has settled a certain distance along the tube, the numerical error accumulates and causes the spheroid to break away from its symmetry plane. While the particle is in the symmetry plane, the forces and torques in the directions, apart from those in which it is supposed to move, are very small. However, once the symmetry is broken, the particle deviates from its expected trajectory. Furthermore, its interaction with the sidewall of the tube results in a complex and unpredictable path, as shown in figure 15. While in the symmetry plane, the particle only rotates about the z-axis. However, the breakage of symmetry results in the rotation of the particle about the other axes too.

This chaotic motion is not the result of numerical errors, but is inherent to the geometry and physics of the system. Further simulations of unconstrained ellipsoids in Stokes flow reveal that when the ellipsoids are released off-centre in non-symmetrical configurations, the motion is similar to that shown in figure 15, in that the motion is generally non-periodic, unpredictable and highly sensitive to changes in the initial configuration. One such case is illustrated in figure 16.

5.4. *Motion of a spheroid at low and moderate Reynolds numbers*

This section discusses the motion of a spheroid falling in an infinitely long tube at finite Reynolds numbers. The fluid inertia leads to a change in the long-term behaviour of the spheroid. In our simulations, we fixed the density ratio $\rho_p/\rho_f = 1.5$. As a first step towards understanding the forces and torques experienced by a spheroid in non-zero Reynolds-number flows, simulations of a falling spheroid in an infinite medium have been performed. A spheroid, constrained to fall vertically without rotation, is released from rest and allowed to fall until it reaches its terminal velocity. At this velocity, the torque and the horizontal forces acting on the spheroid are recorded and shown in figure 17. To achieve the effect in an infinite medium, the ellipsoid is placed inside a cylinder of large radius ($=32a$). It is seen numerically that any further increase in the cylinder diameter causes no perceptible change in the flow field. The notion of the infinite tube is achieved in a similar way to the case of Stokes flow with the inlet and exit of the tube at a distance of $80b$ away from the spheroid.

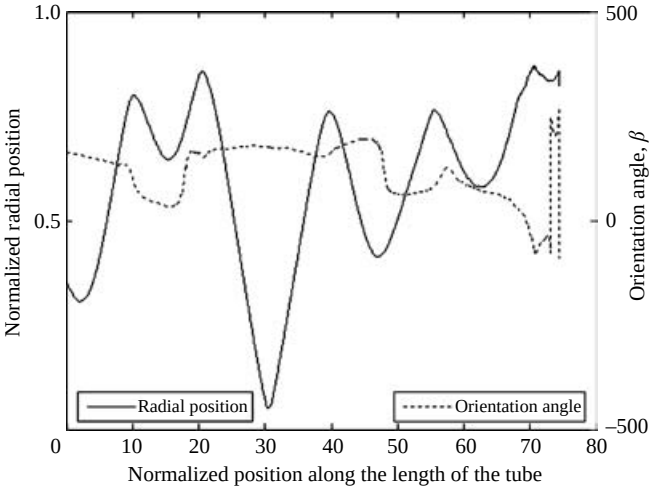

FIGURE 16. Motion of an inertialess unconstrained spheroid falling in a tube under Stokes flow conditions. Initial orientation of the spheroid is $\beta = -15°$. The centre of the spheroid is off-centre from the axis of the tube by a distance of 1.0 in the both the y- and z-directions. The aspect ratio of the spheroid is $a/b = 2.0$.

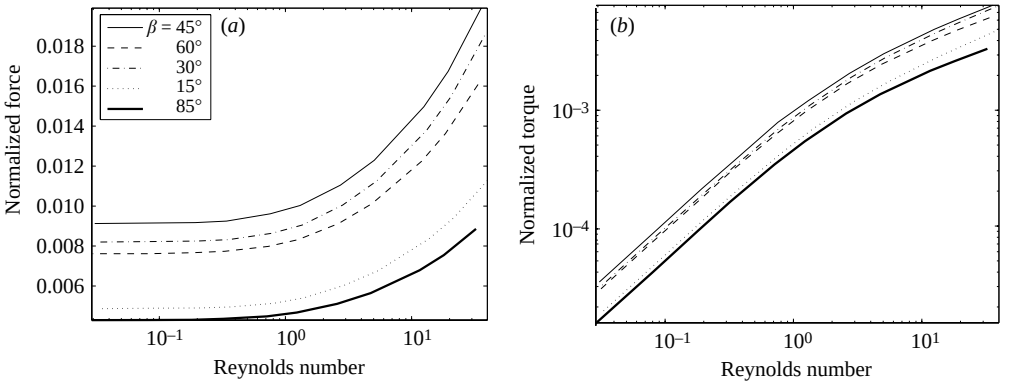

FIGURE 17. Variation of the lateral force and torque experienced by a spheroid, constrained to settle vertically without rotation, as a function of its orientation and the Reynolds number. The force has been normalized with $Vg(\rho_p - \rho_f)$, and the torque with $Vag(\rho_p - \rho_f)$, where V is the volume of the spheroid.

At the symmetric orientations ($\beta = 90°$ and $\beta = 0°$), the values of the lateral force and torque are identically zero. In between these two orientations, both the lateral force and the torque are seen to obtain a highest value near the $\beta = 45°$ configuration. The lateral force and the torque increase with the Reynolds number. The variation seen in figure 17 indicates that near the limit of zero Reynolds number, the torque approaches zero, while the lateral force reaches a plateau, which is as expected. A discussion on the forces acting on a settling ellipsoid in an infinite medium is given in Happel & Brenner (1980, pp. 220–227). The two equilibrium orientations previously mentioned ($\beta = 0°$ and $\beta = 90°$) are classified as unstable and stable, respectively, at non-zero Reynolds numbers. At higher values of Re, vortex shedding occurs and the motion of a spheroid is inherently unsteady, and such a motion is out of the scope of the present study.

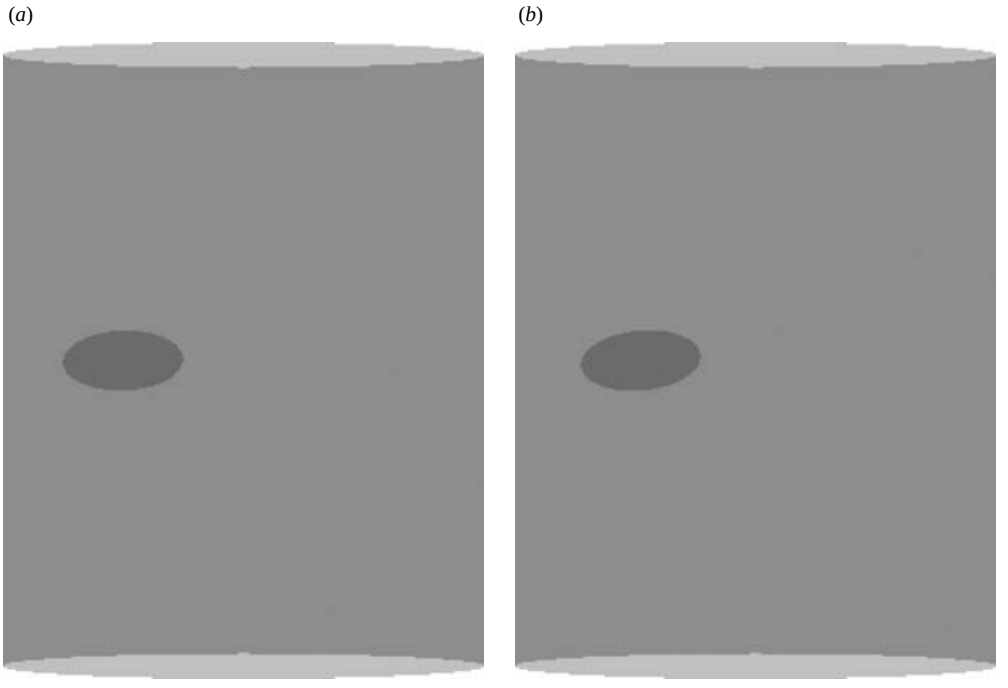

FIGURE 18. Steady-state radial position and orientation for a spheroid settling in a tube at finite Reynolds numbers. The density ratio $\rho_p/\rho_f = 1.5$. The aspect ratio of the spheroid is $a/b = 2.0$ and the tube diameter $D = 8a$. The Reynolds number is changed by adjusting the viscosity of the fluid. (*a*) $Re = 0.3$. (*b*) $Re = 0.9$.

For the case of a spheroid settling in a long tube with a Reynolds number of order $O(1)$, the spheroid reaches a steady-state configuration, wherein it falls vertically with no net force or torque acting on it. This equilibrium configuration is seen to be dependent on the Reynolds number. The locations of this equilibrium for two different values of Reynolds numbers are illustrated in figure 18. Figure 19 plots the path of the centre as well as the orientation of a spheroid as it settles in an infinitely long tube.

The variation of the equilibrium position and orientation as functions of the Reynolds number is shown in figure 20. As previously stated, there are no steady-state positions for $Re = 0$. Unsteadiness sets in at higher Reynolds numbers owing to vortex shedding.

The location of the radial equilibrium position can be explained by examining the two contributions to the torque acting on the spheroid. These two contributing factors are the 'restoring torque' due to fluid inertia which tends to turn the particle perpendicular to the gravity, as seen in figure 17, and the 'reverse-contact torque' due to the bounding wall, as in figure 7. Clearly these two torques, when the spheroid is in equilibrium, will be equal and opposite. If the orientation of the spheroid is fixed, as the Reynolds number increases, the restoring torque is seen (from figure 17) to increase. To balance this increase, the spheroid must move radially inward such that the value of the reverse-contact torque increases accordingly as shown in figure 7. Therefore, with an increase in Re, the equilibrium radial position of the spheroid is expected to decrease. Naturally, at this equilibrium location, the lateral forces acting on the spheroid are also in balance. The force directing the particle towards the wall

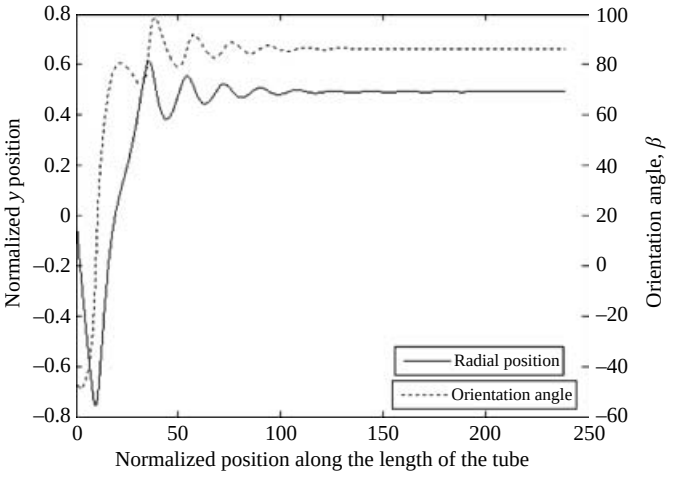

FIGURE 19. Transient motion of a sedimenting spheroid in a tube. The spheroid translates in the (x, y)-plane and rotates about the z-axis. The Reynolds number is 0.6. The normalization is with the tube radius.

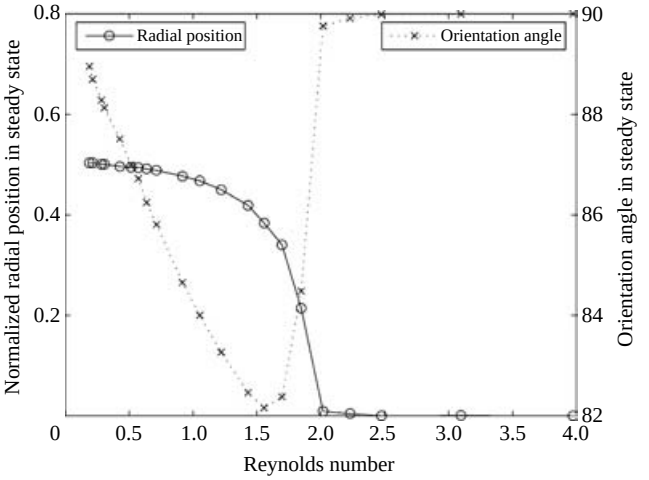

FIGURE 20. Radial position and orientation of a spheroid in its equilibrium steady-state configuration as a function of the Reynolds number of the flow. The radial position is normalized with the tube radius. The aspect ratio of the spheroid is $a/b = 2.0$.

is similar to that seen in figure 17. An inward force due to the sidewall counters this force for equilibrium. These two forces can be termed as 'long-body force' and 'wall force', respectively. For a fixed orientation and Reynolds number, it can be expected that the wall force will decrease as the distance between the spheroid and the wall increases. Figure 17 shows that at around $Re = 2$, there is a rapid increase in the long-body force. Since, as shown above, a balance of torques requires that the spheroid be not close to the wall at such a value of Reynolds number, the wall-force is unable to balance the long-body force at any orientation other than at $\beta \sim 90^\circ$, where the long-body force itself is very small. At the horizontal orientation, $\beta \sim 90^\circ$, the restoring torque is also very small. Hence, the reverse-contact torque must also be very

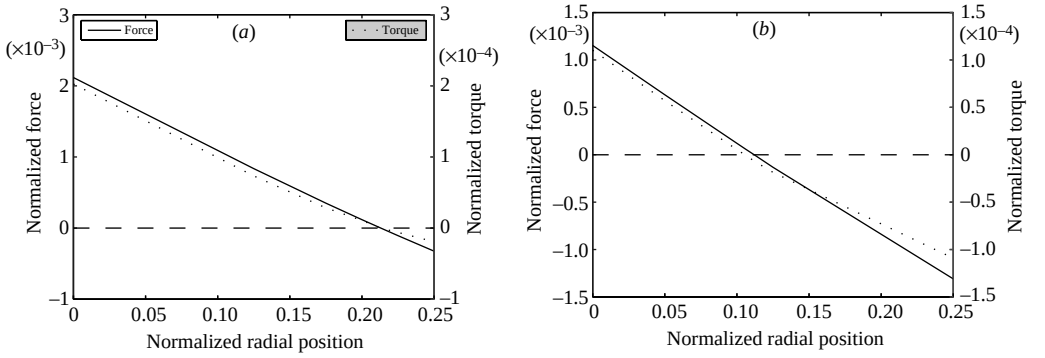

FIGURE 21. Forces and torques acting on a spheroid, constrained to sediment vertically without rotation in an infinitely long tube, as a function of its radial position inside the tube at two different orientations. The equilibrium radial position for this Reynolds number is 0.21, and the equilibrium orientation is $\beta = 84.5°$. The radial position has been normalized with the tube radius. (*a*) $\beta = 84.5°$. (*b*) $\beta = 87°$.

small which is achieved when the spheroid is at the centre of the tube. This change in the behaviour corresponds to the sharp decrease in the equilibrium radial position seen in figure 20. The observation that the particle achieves a steady equilibrium at the centreline of the tube, with a horizontal orientation, agrees with the results from Feng *et al.* (1994) for the case of a sedimenting two-dimensional elliptic cylinder between parallel walls at similar values of the Reynolds number. They observed that this equilibrium becomes unstable at Reynolds number around 25. The oscillatory motion described in that study, upon further increase in the Reynolds number, should also occur here for the three-dimensional situations. However, they missed the stable equilibrium configurations, off the centreline of the tube, for particle Reynolds numbers less than 2.0. Aidun Lu & Ding (1998) used the lattice-Boltzmann method to study ellipsoids settling in an infinite channel and also reported the presence of torque-free equilibrium positions.

To verify the location of the equilibrium configuration, the force and torque acting on the spheroid at $Re = 1.85$, have been recomputed when the spheroid is perturbed from its equilibrium position and orientation. Results of those calculations are shown in figure 21. The spheroid is constrained to fall vertically without rotation, at its equilibrium orientation of $\beta = 84.5°$. The force and torque are noted as a function of the radial position of the particle inside the tube. It can be seen, from figure 21(*a*), that the both the force and torque become identically equal to zero only at the equilibrium radial position of 0.21. Also from figure 21(*b*), it is evident that for an orientation, which is different from the equilibrium one of $\beta = 84.5°$, there exists no position where both the force and torque are zero, implying that for this particular Reynolds number, only one combination of position and orientation is possible for the equilibrium.

The dependence of the equilibrium position and orientation of the spheroid as functions of its aspect ratio has also been examined. The results are shown in figure 22. In many ways, the effect of an increase in the aspect ratio is similar to an increase in the Reynolds number. Both lead to a rise in the long-body force and the restoring torque. The argument, showing why an increase in Reynolds number caused a decrease in the equilibrium radial position (seen in figure 20), is thus similarly applicable to an increase in the aspect ratio. The balance of torques (restoring and

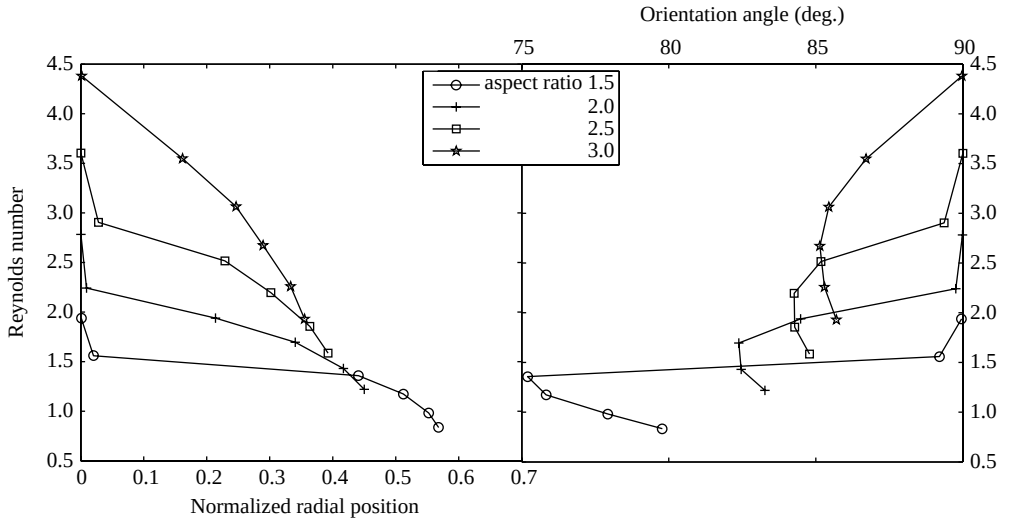

FIGURE 22. Variation of equilibrium position and orientation for different values of aspect ratio of the spheroid. The radial position has been normalized with the tube radius. The density ratio $\rho_p/\rho_f = 1.5$ and the tube diameter $D = 16b$. The aspect ratio is changed by adjusting the value of a.

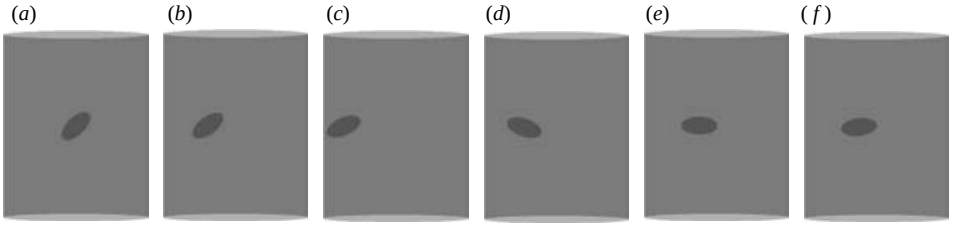

FIGURE 23. Transient motion of a spheroid settling in a tube at a Reynolds number around 1.0. Initial orientation of the spheroid is $\beta = -45^\circ$. The aspect ratio of the spheroid is $a/b = 2.0$ and the tube diameter $D = 8a$. The density ratio $\rho_p/\rho_f = 1.5$.

reverse-contact) will require that as the aspect ratio of the spheroid is increased, the reverse-contact torque also be increased, and hence, the radial equilibrium position moves inward. Variations to this general rule may occur depending on the equilibrium orientation angle (β at equilibrium will not be the same for different aspect ratios).

Since the spheroid has been constrained to move in its symmetry plane, it reaches its equilibrium configuration without any rotation with respect to the x- or y-axis. However, by symmetry considerations, it is easy to see that there exist an infinite number of radially symmetric positions of equilibrium wherein the orientation of the body will be different with respect to the given fixed coordinate system, but will essentially be the same when considering the y-axis as being along the radial direction from the axis of the tube to the centre of the body with the x-axis being along the direction of gravity. The motion that the particle undergoes to reach this orientation is shown in figure 23 for a particular Reynolds number.

Figure 24 shows the transient path of the centre of a spheroid which settles in an infinite tube at various Reynolds numbers. All the paths eventually reach equilibrium

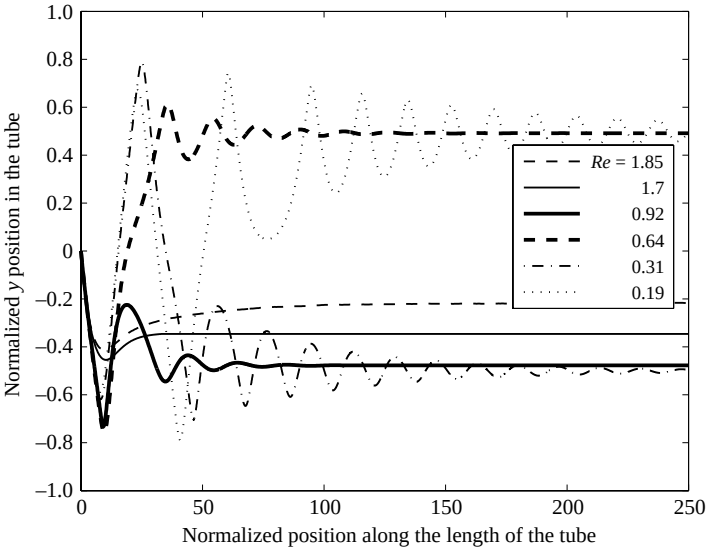

FIGURE 24. The motion of the centre of an ellipsoid settling in a long tube seen at various Reynolds numbers. The particle centre initially lies along the axis of the tube and the initial orientation angle $\beta = -45^\circ$. The normalization is with the tube radius.

states. It should be noted that while the final position may correspond to a positive (right-hand side of tube) or negative (left-hand side of tube) value on the y-axis, only the absolute value of y (the radial position) is of significance. As the Reynolds number is reduced, it has been shown that the torque tilting the spheroid towards the horizontal configuration drops accordingly (figure 17), and the spheroid oscillates from side to side when it is not in the horizontal configuration (seen in figure 5). Hence, the combined effect of these two is to produce a motion wherein the spheroid oscillates from one side to another until it reaches its equilibrium configuration. The distance travelled by the spheroid before it settles into equilibrium, increases with reducing Reynolds numbers. Moreover, it can be seen that the two configurations of an ellipsoid with its centre on the axis of the tube and oriented at $\beta = 90^\circ$ and $\beta = 0^\circ$ are not always the stable equilibriums in this Reynolds number regime.

5.5. *Asymmetric motion of a spheroid at finite Reynolds numbers*

The existence of stable equilibrium configurations of a spheroid in flows at low and intermediate Reynolds numbers, as opposed to the lack thereof in Stokes flow, markedly differentiates the behaviour of an unconstrained spheroid in the two cases. While its motion in the case of Stokes flow is seen to be almost random (figure 15), its long-term configuration in the case of finite Reynolds numbers is the achievement of one of the symmetrically equivalent equilibrium states. Figure 25 presents the orientation of a unconstrained spheroid settling in a tube under three different initial conditions. This figure demonstrates that irrespective of the initial configuration, even from an asymmetric starting configuration, the spheroid eventually settles into one of the equivalent equilibrium states. It can thus be concluded that these equilibrium positions are globally stable.

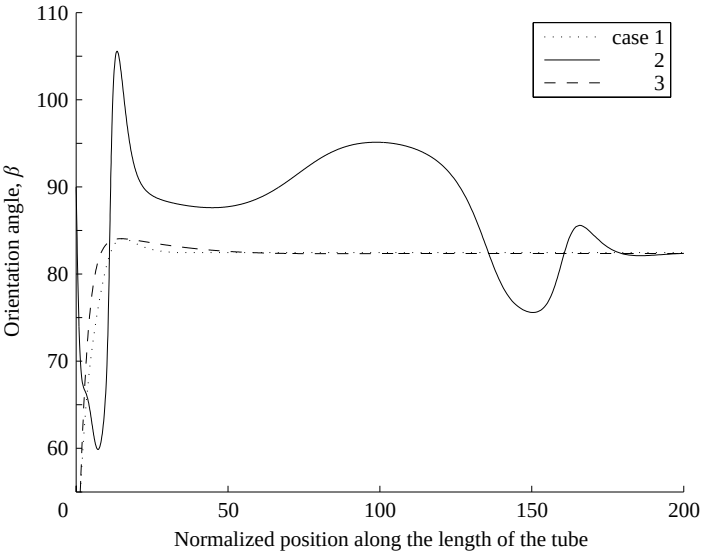

FIGURE 25. Variation of the orientation angle with position along the length of a tube for a freely falling spheroid. The three cases correspond to three different initial starting positions. Case 1: constrained motion with initial $y = z = 0$ and $\beta = 45°$. Case 2: unconstrained motion with initial $y = 0$, $z = 1$ and $\beta = 90°$. Case 3: unconstrained motion with initial $y = z = 0$ and $\beta = 45°$. The Reynolds number is 1.7, and the aspect ratio of the spheroid is 2.0.

6. Conclusions

The following conclusions can be drawn about the motion of a spheroid settling in an infinitely long tube.

(i) For the case of an inertialess spheroid under Stokes flow conditions, its motion is found to be perfectly periodic, as expected, in which the spheroid rotates and moves from side to side in the tube as it settles. The amplitude and the period of this oscillatory motion depend on the initial orientation and the aspect ratio of the spheroid.

(ii) For the case of a spheroid with inertia under Stokes flow conditions, its motion is found initially to follow a similar oscillatory orbit with an increasing amplitude. Its orientation tends towards a more flat (horizontal) configuration, and the rate of change of its orientation increases with the particle Stokes number. The spheroid eventually collides with the tube wall, and settles into a stable periodic orbit.

(iii) For the case of a spheroid in finite-Reynolds-number flows, it eventually reaches a steady-state configuration wherein it falls vertically. The location and configuration of this steady equilibrium varies with the Reynolds number.

This work was supported, in part, by grants from The Research Foundation of the University of Pennsylvania, and from the Defense Advanced Research Project Agency (DARPA). K. M. would also like to acknowledge NASA for their support under grant number NAG9-1400.

REFERENCES

AIDUN, C. K., LU, Y. & DING, E. 1998 Direct analysis of particulates with inertia using the discrete Boltzmann equations. *J. Fluid Mech.* **373**, 287–311.

BRODAY, D., FICHMAN, M., SHAPIRO, M. & GUTFINGER, C. 1998 Motion of spheroidal particles in vertical shear flows. *Phys. Fluids* **10**, 86–100.

Caswell, B. 1972 The stability of particle motion near a wall in newtonian and non-Newtonian fluids. *Chem. Engng Sci.* **27**, 373–389.

Chou, J. C. K. 1992 Quaternion kinematic and dynamic differential equations. *IEEE Trans. Robot. Automat.* **8**, 53–64.

Cox, R. G. 1965 The steady motion of a particle of arbitrary shape at small Reynolds numbers. *J. Fluid Mech.* **23**, 625–643.

Feng, J., Hu, H. H. & Joseph, D. D. 1994 Direct simulation of initial value problems for the motion of solid bodies in a newtonian fluid. Part 1. Sedimentation. *J. Fluid. Mech.* **261**, 95–134.

Happel, J. & Brenner, H. 1980 *Low Reynolds Number Hydrodynamics.* Martinus Nijhoff.

Hu, H. H. 1996 Direct simulation of flows of solid–liquid mixtures. *Intl J. Multiphase Flow* **22**, 335.

Hu, H. H., Joseph, D. D. & Crochet, M. 1992 Direct simulation of fluid particle motions. *Theoret. Comput. Fluid Dyn.* **3**, 285–306.

Hu, H. H., Patankar, N. & Zhu, M. 2001 Direct numerical simulations of fluid–solid systems using arbitrary-Lagrangian–Eulerian technique. *J. Comput. Phys.* **169**, 427–462.

Jeffery, G. B. 1922 The motion of ellipsoidal particles immersed in a viscous fluid. *Proc. R. Soc. Lond.* A **102**, 161.

Kuipers, J. 1999 *Quaternions and Rotation Sequences.* Princeton University Press.

Liu, H., Bau, H. H. & Hu, H. H. 2004 On the translation of a cylinder in a long tube. *Phys. Fluids* **16**, 998–1007.

Liu, Y. J., Nelson, J., Feng, J. & Joseph, D. D. 1993 Anomalous rolling of spheres down an inclined plane. *J. Non-Newtonian Fluid Mech.* **50**, 305–329.

Pan, T. W., Glowinski, R., Joseph, D. D. & Bai, R. 2003 Direct simulation of the motion of settling ellipsoids in newtonian fluid. *Fourteenth Intl Conf. on Domain Decomposition Methods.*

Russel, W. B., Hinch, E. J., Leal, L. G. & Tieffenbruck, G. 1977 Rods falling near a vertical wall. *J. Fluid Mech.* **83**, 273–287.

Sugihara-Seki, M. 1993 The motion of an elliptic cylinder in channel flow at low Reynolds numbers. *J. Fluid Mech.* **257**, 575–596.

Sugihara-Seki, M. 1996 The motion of an ellipsoid in tube flow at low Reynolds numbers. *J. Fluid Mech.* **324**, 287–308.

Wakiya, S. J. 1957 Viscous flows past a spheroid. *J. Phys. Soc. Japan* **12**, 1130–1141.